RSC Advances

PAPER

View Article Online
View Journal | View Issue

Cite this: *RSC Adv.*, 2021, **11**, 19656

Effects of pendant side groups on the properties of the silicon-containing arylacetylene resins with 2,5-diphenyl-[1,3,4]-oxadiazole moieties†

Manping Ma, Xiaotian Liu, Chuan Li, Zhiyao Qiao, Qiaolong Yuan and Farong Huang *

Received 19th March 2021
Accepted 23rd May 2021

DOI: 10.1039/d1ra02184b

rsc.li/rsc-advances

Silicon-containing arylacetylene resins with rigid conjugated structures in the main chain often exhibit poor processability. A strategy of improving the processability by destroying the molecular structure symmetry using side aromatic groups was proposed, and the effects of the side groups was further explored. Two novel structural resins with side aromatic phenyl and phenylacetylene groups (PODSA-2P-MM and PODSA-2E-MM) were synthesized by Grignard reaction. The side aromatic groups strongly interfere with the regular arrangement of the main chains, and the crystallinities of the resins decrease as compared with PODSA-MM resin without side aromatic groups. Due to the influence of the side aromatic groups, the novel resins exhibit good processability, low exothermic enthalpy, high modulus and good heat resistance.

Introduction

Thermosetting resins have been widely used in various aspects of our society.[1–3] As types of high-performance thermoset resins, silicon-containing arylacetylene resins, which have high heat-resistance, excellent dielectric properties, low water uptake, high-temperature ceramic properties and good mechanical properties, are known and they have potential applications in the aerospace and defense fields.[4–9] Brittleness is one of the disadvantages of thermosetting resins, and silicon-containing arylacetylene resins are no exception.[4,9] To solve this problem, polar aromatic ether structures and siloxane structures were introduced into the resins to modify the toughness of the resins.[10–14] Huang's group prepared a series of silicon-containing arylacetylene resins with polyphenylene oxide segments in the main chain, which show good mechanical properties.[14–16] With the increase of the polyphenylene oxide segments in the main chain, the mechanical properties of the resins gradually increase, but processability and heat resistance gradually deteriorate. Thereafter, we introduced the rigid-rod 2,5-diphenyl-[1,3,4]-oxadiazole into silicon-containing arylacetylene resin to obtain the PODSA resins with high mechanical properties and thermal relaxation temperatures. However, their processabilities were not very good.[17]

The properties of polymers depend largely on their chemical structures. Many researchers improved the processabilities of the resins by introducing side groups into the main chains.[18,19] Lenz and co-workers[19] found that the presence of pendent side groups in main chains of a thermotropic liquid crystalline polymer (TLCP) decreased both melting point and clearing temperature. Han team[20] investigated the rheological behaviors of TLCP by changing the volume of side groups, and found that polymers with larger side groups had lower viscosity, which demonstrated that the pendent side groups played a significant role in determining the rheological properties of a polymer. In addition, Dingemans group[21] introduced a phenylethynyl group into side positions of semicrystalline poly(decamethylene terephthalamide) (PA 10T) to get a high-temperature shape-memory polymer, and the produced polymer showed lower melting temperature and exothermic enthalpy as compared with PA 10T. At same time, the glass relaxation temperature gradually decreased with the concentration of the functionalized side group.

In this work, to explore the effects of side aromatic groups on the properties of a silicon-containing arylacetylene resin, the phenyl and phenylacetylene groups were introduced. We prepared three novel resins (PODSA-MM, PODSA-2P-MM, PODSA-2E-MM) by Grignard reactions of 2,5-bis-(4-ethynylphenoxy)-[1,3,4]-oxadiazole, 2,5-bis(6-(4-ethynylphenoxy)-[1,1′-biphenyl]-3-yl)-[1,3,4]-oxadiazole, 2,5-bis(4-(4-ethynylphenoxy)-3-(phenylethynyl)phenyl)-[1,3,4]-oxadiazole with dimethyldichlorosilane, respectively.[14] The morphology, processability, thermal behaviors, thermal and mechanical properties of these resins were investigated in detail.

Key Laboratory for Specially Functional Materials and Related Technology of the Ministry Education, School of Materials Science and Engineering, East China University of Science and Technology, Shanghai 200237, China. E-mail: fhuanglab@ecust.edu.cn

† Electronic supplementary information (ESI) available. See DOI: 10.1039/d1ra02184b

Results and discussion

Synthesis and characterization of the resins

As shown in Scheme 1, the resins were prepared with the ratio of aromatic diynes to silane of 3 : 2. 2,5-Bis-(4-ethynylphenoxy)-[1,3,4]-oxadiazole reacted with dimethyldichlorosilane by Grignard reactions to get PODSA-MM. Similarly, PODSA-2P-MM and PODSA-2E-MM were prepared by the replacement of 2,5-bis-(4-ethynylphenoxy)-[1,3,4]-oxadiazole with 2,5-bis(6-(4-ethynylphenoxy)-[1,1′-biphenyl]-3-yl)-[1,3,4]-oxadiazole and 2,5-bis(4-(4-ethynylphenoxy)-3-(phenylethynyl)phenyl)-[1,3,4]-oxadiazole, respectively. The resins are yellow solid and soluble in common solvents such as THF, toluene and dichloromethane (see Table 1). Take PODSA-2E-MM as an example, the chemical structure of resin was characterized by proton nuclear magnetic resonance (^{1}H-NMR) spectroscopy, Fourier transform infrared (FT-IR) spectroscopy and gel permeation chromatography (GPC) analyses. As shown in Fig. 1, the signals at the range of 7.0–8.5 ppm correspond to the hydrogen of aromatic rings in the resin. The signal (a) at 3.05 ppm belongs to the hydrogen of terminal acetylene groups. The peak (b) at 0.49 ppm is ascribed to the signal of Si–CH_3, attributing to that the silane unit was introduced into the resin chain. And the integral area ratio of the peaks at position (a) and (b) is 1.00 : 5.80, which is close to the design value 1.00 : 6.00, demonstrating that the resin has been synthesized successfully. As shown in Fig. 1A, with the presence of side aromatic groups, the signals at (e) and (f) in 2,5-diphenyl-[1,3,4]-oxadiazole structure have been little change, the signal at position (g) moves from 8.10 ppm for BEPOD to 8.20 ppm for BEPOD-2P and then 8.35 ppm for BEPOD-2E. The results indicate that the large conjugated structures between substituted phenyl or phenylacetylene group and 2,5-diphenyl-[1,3,4]-oxadiazole structure affect the electron cloud of corresponding aromatic ring.[22] In addition, the signals at position (d) moves from 7.02 ppm for BEPOD to 6.90 ppm for BEPOD-2P and then 7.04 ppm for BEPOD-2E, which could be attributed to that the adjacent side phenyl groups interfere with the spatial arrangement of benzenes with terminal acetylene groups, but the side phenylacetylene groups hardly cause the phenomena. The change of signal at position (a) is similar with that of position (d). The signal at position (c) shows little movement. Similarly, these shift phenomena also occur in the ^{1}H-NMR spectra of corresponding resins. In addition, the vibration signal of Si–CH_3 moves from 0.40 ppm for PODSA-MM to 0.46 ppm for PODSA-2P-MM and then 0.49 ppm for PODSA-2E-MM.

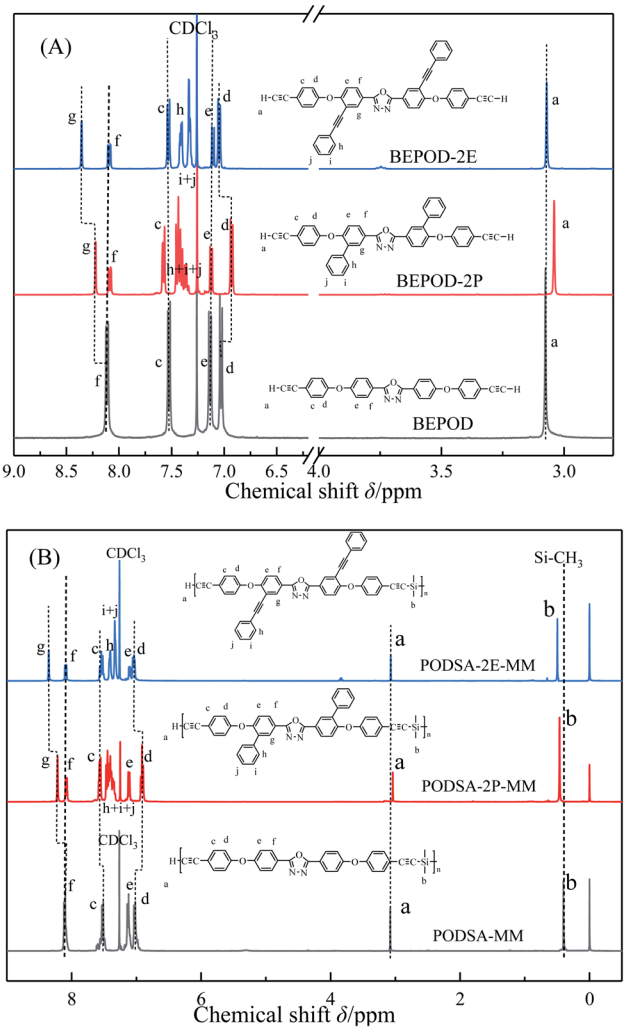

Fig. 1 The ^{1}H-NMR spectra of diynes (A) and aromatic resins (B) in $CDCl_3$-d.

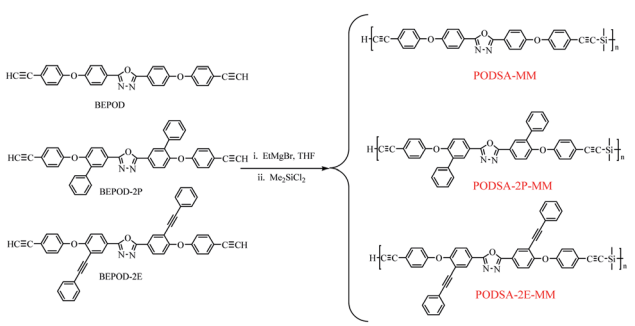

Scheme 1 The synthetic route of the silicon-containing arylacetylene resins.

As can be seen from Fig. 2, the peak at 3288 cm^{-1} is assigned to the stretching vibration of ≡C–H, the peak at 3056 cm^{-1} is Ar–H stretching vibration absorption of benzene ring, the C–H vibration signal of Si–CH_3 is 2965 cm^{-1}. The peak at 2156 cm^{-1} is assigned to the characteristic absorption of Ar–C≡C–Si in the mainchain of PODSA-2E-MM, and the absorption peak at 2220 cm^{-1} is the signal of Ar–C≡C–Ar in the side position of PODSA-2E-MM. The signals at 1610 and 1594 cm^{-1} correspond to the [1,3,4]-oxadiazole. The peaks at 1250 cm^{-1}, 1224 cm^{-1} and 790 cm^{-1} are attributed to the vibration signals of Si–CH_3, Ar–O–Ar and Si–C≡C, respectively. In addition, the absorption of –C≡C– and [1,3,4]-oxadiazole move from 2159 and 1613 cm^{-1} for PODSA-MM to 2156 and 1612 cm^{-1} for PODSA-2P-MM and then 2156 and 1610 cm^{-1} for PODSA-2E-MM, respectively. The trends move towards low wavenumbers, which could be attributed to that steric hindrance effects of side aromatic groups. The absorption of ≡C–H and Si–CH_3 move towards high wavenumber show that the movement of these

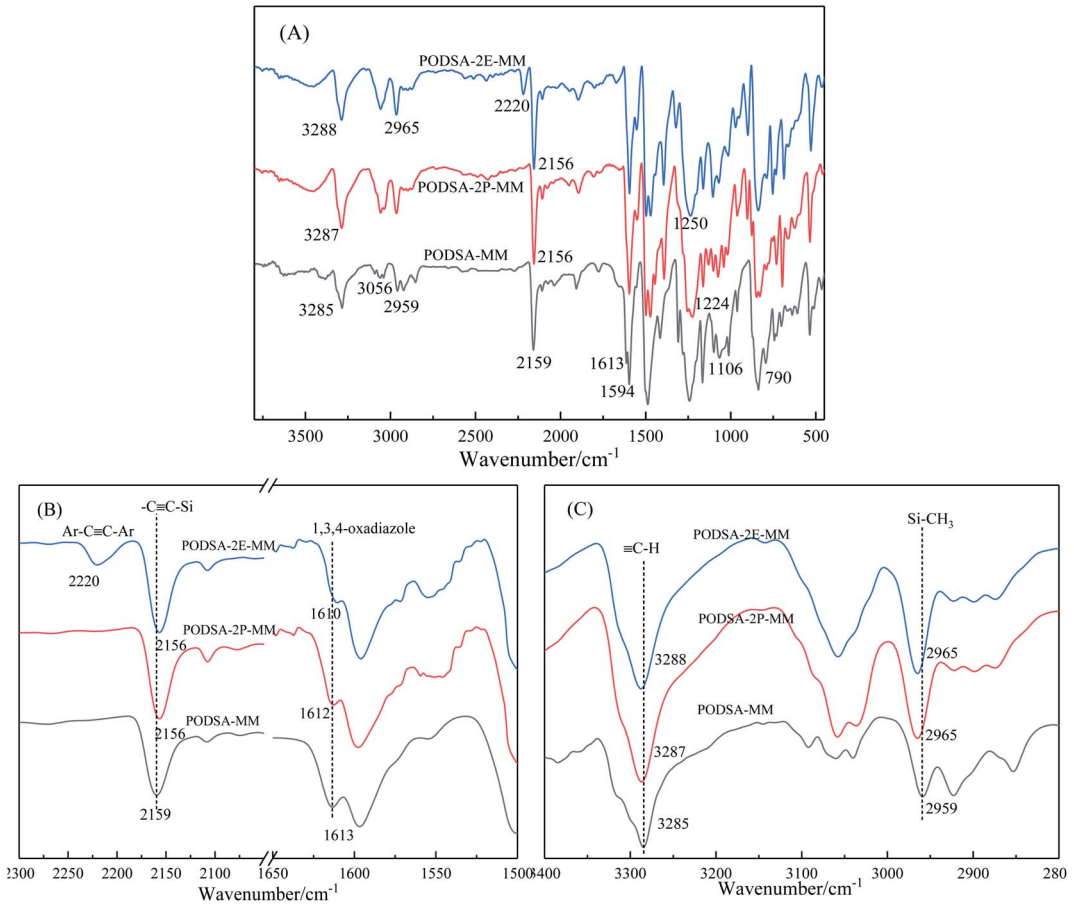

Fig. 2 The FT-IR spectra of three PODSA resins full range (A), in the range of 1500–2300 cm^{-1} (B) and in the range of 2800–3400 cm^{-1} (C).

Table 1 The solubility of resins[a]

Solvent	DMF	THF	EtOH	Acetone	CH_3CN	CH_2Cl_2	Toluene	Petroleum ether
PODSA-MM	++	++	–	+	+	++	+	–
PODSA-2P-MM	++	++	–	++	++	++	++	–
PODSA-2E-MM	++	++	–	++	++	++	++	–

[a] Note: ++: soluble; +: partially soluble; –: insoluble.

groups increase. These results are consistent with the results of ^{1}H-NMR spectra.

The relative molecular weights of three resins measured by GPC were listed in Table 2. The $\overline{M_n}$ and PDI of resins are close to the designed value, and three resins have similar molecular weight and distribution.

Table 2 The GPC data of three PODSA resins

Resin	$\overline{M_n}$	$\overline{M_w}$	PDI
PODSA-MM	1508	2698	1.78
PODSA-2P-MM	1555	2766	1.78
PODSA-2E-MM	1677	3121	1.86

The effects of side groups on the PODSA resins

Optical properties of resin solutions. The change of structure could lead to the change of optical properties for aromatic polymers. The optical properties of three PODSA resin solutions were investigated by UV-Vis absorption and fluorescence emission spectra. The UV-Vis absorption spectra of three resin solutions show similar phenomena. There are maximum absorption peaks at 247 nm and 297 nm with shoulders and fine structures attributed to the π–π* relaxation of aromatic structures.[23] The wide shoulders are mainly due to interchain π-orbital overlap. The UV-Vis absorption shoulders of three resin solutions don't have significant difference except slight red-shift phenomena, indicating the almost similar interchain π-orbital overlap. The substituted phenyl and phenylacetylene

groups on the 2,5-diphenyl-[1,3,4]-oxadiazole unit make the intrachain charge-transfer interactions between the electron-withdrawing units and the electron-donating units more intense due to π-electron delocalization, leading to that the resin solution show slight red-shift phenomena in both UV-Vis and fluorescence spectra.[24] At the same concentration, the fluorescence emission intensity of the resin solution decreased due to the presence of the side groups (excited wavelength: 220 nm). Because of the presence of side aromatic groups, intramolecular charge-transfer interactions were enhanced due to π-electron delocalization, but the restrictions of molecular structures caused by the π–π stacking interactions are weakened due to the deflection of the side groups to the [1,3,4]-oxadiazole units (Fig. S2†), leading to that the molecular vibration caused by the excited electrons are enhanced. The part of excitation energy is dissipated in the form of heat energy caused by vibration, leading to the decrease of fluorescence intensities of resin solutions (Fig. 3).[25]

The morphologies of the resins. The difference of crystallinity of PODSA-MM resins before and after introducing side group were investigated by X-ray diffraction (XRD) analysis at the range of 5°–50°. The results are shown in Fig. 4A. Three resins are partially crystalline state at room temperature due to long-period ordered structures of molecular chains. The crystallization peaks at 19.3°, 23.6° and 28.6° for PODSA-MM resin were not observed on the XRD curves of PODSA-2P-MM and PODSA-2E-MM resins, which are attributed to the long-period ordered structures disturbed due to the deflection of side aromatic groups to rigid 2,5-diphenyl-[1,3,4]-oxadiazole. Accordingly, the three-dimensional structure of the aromatic diynes at the lowest energy states show that the deflection of the side groups to the 2,5-diphenyl-[1,3,4]-oxadiazole unit. The larger the volume of side group, the larger the deflection angle (Fig. S2†). This indicates that the side aromatic groups hinder the crystallization of the molecular chains. In addition, by comparing the crystallization phenomena of PODSA-2P-MM and PODSA-2E-MM resins, it is found that XRD of PODSA-2E-MM resin has a slight bulge at about 25°, which may be attributed to the ordered arrangement of rigid deflective phenylacetylene groups.[26]

The disorder degrees of molecular chains increase with the appearance of side group, and the disorder degrees become

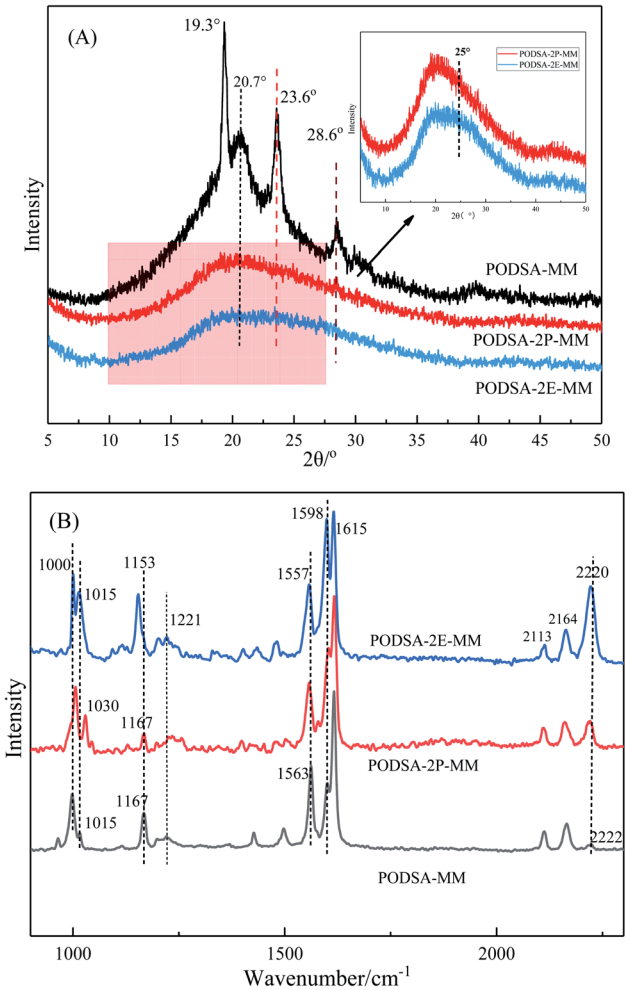

Fig. 4 The XRD diagrams (A) and Raman spectra (B) of three PODSA resins.

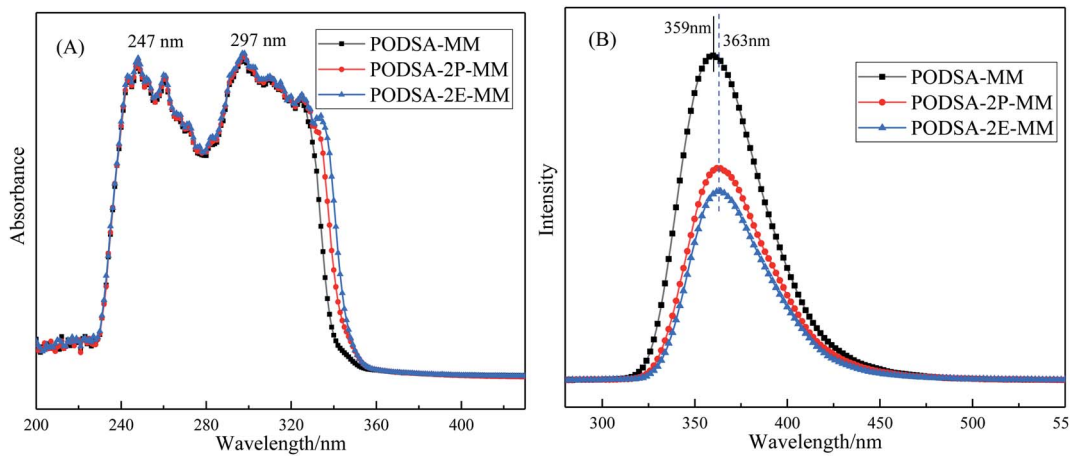

Fig. 3 The UV-Vis (A) and fluorescence (B) spectra of three PODSA resin solutions (THF, 2×10^{-5} mol L^{-1}).

more severe with the increase of side group volume. The microstructure of resin was further investigated by laser Raman scattering analysis, the results are shown in Fig. 4B. There are obvious changes in these peaks at about 1000 cm^{-1}, 1015 cm^{-1}, 1221 cm^{-1}, 1557 cm^{-1}, 1598 cm^{-1} and 2220 cm^{-1}, but the intensities are different. The peaks at 1000 cm^{-1} and 1221 cm^{-1} corresponds to the vibration of C–O–C and Ar–O–Ar, respectively. The peaks at about 1015 cm^{-1} and 1153 cm^{-1} correspond to the vibration of C–H for aromatic rings, the signals at about 1557 cm^{-1}, 1598 cm^{-1} and 1615 cm^{-1} are assigned to the [1,3,4]-oxadiazole and skeleton of benzene.[27] The peak at 2220 cm^{-1} is ascribed to the vibrational signal of the internal acetylene groups in resins. The percentage of internal acetylene groups is the order of PODSA-2E-MM > PODSA-MM > PODSA-2P-MM. However, the Raman intensity of PODSA-2P-MM is higher than that of PODSA-MM, indicating that the vibrations of bonds were reinforced. With the presence of side aromatic groups, the many vibrational peaks become stronger even have slight shifts, indicating that the disorder degrees of structures increase.[28] The results are consistent with the fact that the crystallinity of the resins become worse and the part of the excitation energy is dissipated by molecular vibration in fluorescence spectroscopy.

The rheological properties of the resins. The rheological properties of resins were explored by rotational rheological test, and the results are shown in Fig. 5. In general, the processability of thermosetting resin depends on the structure of resin. The viscosity–temperature curves of three resins show obviously different rheological properties. As the volumes of side aromatic groups increase, the melting temperatures of resins increase in the order of PODSA-2E-MM < PODSA-2P-MM < PODSA-MM, and the temperatures of gel point (T_{gel}) move towards high temperature, which should be attributed to low content of terminal acetylene groups disturbed by side aromatic groups.[17] The processing windows of resins widen in the order of PODSA-2E-MM > PODSA-2P-MM > PODSA-MM, showing that the processabilities of the resins are getting better due to the presence of side aromatic groups. There is a slow viscosity-decreasing process near melting temperature in the viscosity–temperature curves of the resins, indicating that the chain mobilities of resins are still restricted by the π–π stacking interactions of 2,5-diphenyl-[1,3,4]-oxadiazole structure. In addition, the larger the volume of side aromatic group is, the wider the range of low viscosity is.

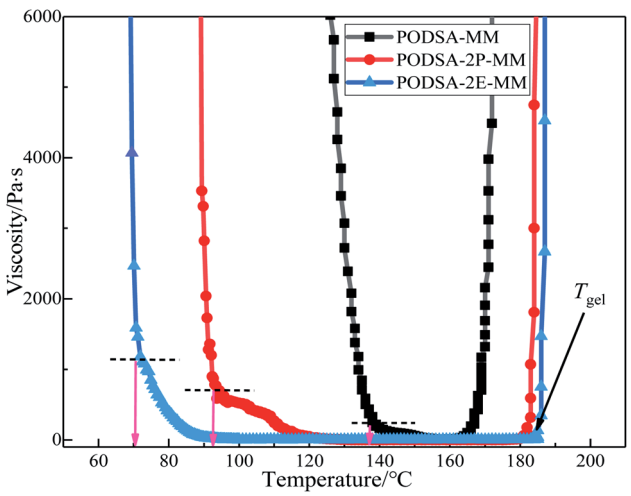

Fig. 5 The viscosity–temperature curves of three PODSA resins.

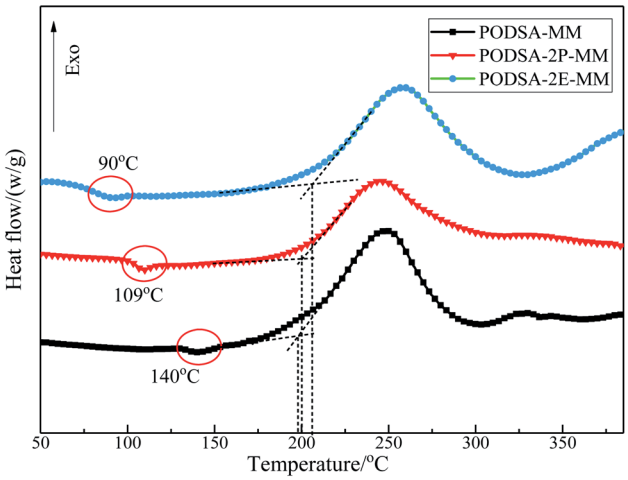

Fig. 6 The DSC curves of three PODSA resins in nitrogen.

The thermal curing behaviors of the resins. The thermal curing behaviors of three resins were investigated by DSC analysis, the results are shown in Fig. 6 and Table 3. Three resins have melting temperature below 150 °C, and large and wide exothermic peak in the range of 200 –300 °C, indicating that the mild thermal cross-linking reactions. With the increase of size of the side aromatic groups, the melting temperatures of resins gradually decrease, while the initial curing temperature (T_i) moves slightly to high temperature. The content of acetylene group in the resins is small due to the side groups, leading to that the exothermic enthalpy (ΔH) of curing reactions decrease. However, the introduction of side phenylacetylene group in PODSA-2E-MM resin increase the value.

The curing kinetics of resins were studied by Kissinger and Ozawa methods.[17] The fitting curves of $\ln(\beta/T_p^2)$ *vs.* T_p^{-1} (Kissinger) and $\ln(\beta)$ *vs.* T_p^{-1} (Ozawa) of three resins are shown in Fig. 7. The apparent reaction activation energy (E_a) of the resin was calculated according to the equations in ref. 17. The E_a of three resins are close and about 100 kJ mol^{-1}, indicating easy thermal crosslinking reactions. The results can be seen in Table 3.

The resins were cured by the process: 170 °C/2 h + 210 °C/2 h + 250 °C/2 h + 280 °C/2 h, and the cured resins were named as PODSA-MM-C, PODSA-2P-MM-C and PODSA-2E-MM-C, respectively. The FT-IR spectra of cured PODSA-2E-MM resin at different temperature are shown in Fig. 8. The reaction degrees of resins were calculated by the ratio of integral area of infrared absorption peak for acetylene groups at 3288 cm^{-1} (C≡C–H), 2200 cm^{-1} (Ar–C≡C–Ar) and 2156 cm^{-1} (Ar–C≡C–Si) before and after curing to that of reference peak for [1,3,4]-oxadiazole at 1610 and 1594 cm^{-1} in FT-IR spectra.[29] The relative conversions (D) of acetylene groups are determined as follows:

Table 3 The DSC data and E_a value of three PODSA resins

Resin	T_i/°C	T_p/°C	T_f/°C	ΔH/(J g^{-1})	E_a/(kJ mol^{-1}) Kissinger method	E_a/(kJ mol^{-1}) Ozawa method
PODSA-MM	198	248	276	463.5	103.0	106.8
PODSA-2P-MM	200	242	297	242.3	96.7	100.1
PODSA-2E-MM	204	256	307	263.5	90.0	94.0

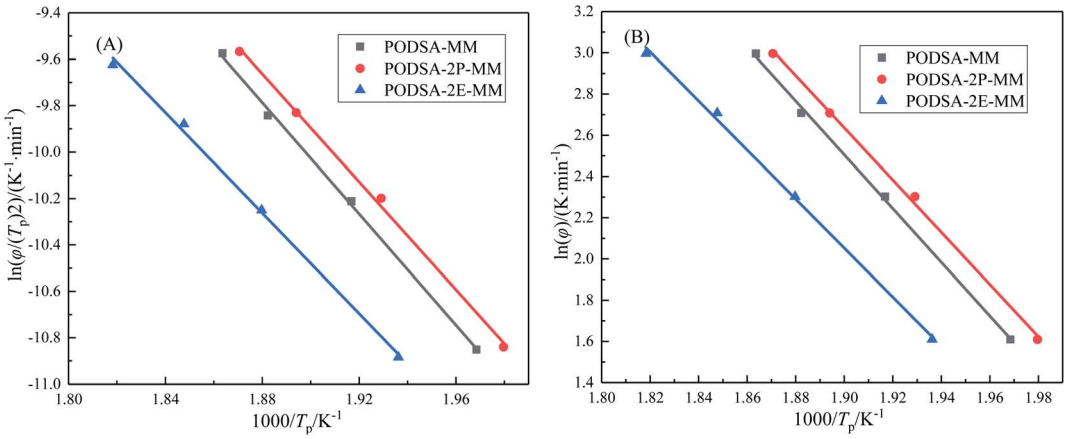

Fig. 7 $\ln(\beta/T_p^2)$ *vs.* T_p^{-1} (A) and $\ln(\beta)$ *vs.* T_p^{-1} (B) plots for the curing of resins.

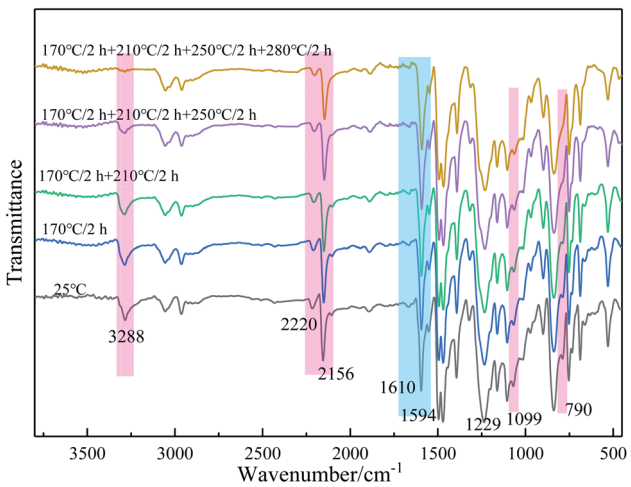

Fig. 8 The FT-IR spectra of PODSA-2E-MM at different temperature.

$$D = \left\{1 - \left[\frac{(A_i/A_0)_a}{(A_i/A_0)_b}\right]\right\} \times 100\%$$

where $(A_i/A_0)_a$ and $(A_i/A_0)_b$ are the ratio of integral area of responding characteristic peak to that of reference peak after curing and before curing, respectively. The reaction degree of resin is shown in Fig. 9. In the process of thermal crosslinking, internal and terminal acetylene groups participate in the reactions.[17] After resins curing, the conversions of terminal acetylene group of three resins are close to 100%, and the conversion of internal acetylene groups in the main chain are about 20%. In addition, the side phenylacetylene group in PODSA-2E-MM participated in the thermal crosslinking reactions in Fig. 9, which lead to that the conversion of internal acetylene groups increase.

The effects of side groups on the cured PODSA resins

The microstructures of the cured resins. The three cured resins obtained by heating show dark reddish networks due to a large number of aromatic structures and thermal crosslinking reactions of acetylene groups. In general, the microstructures of the resins will change after curing because of the crosslinking

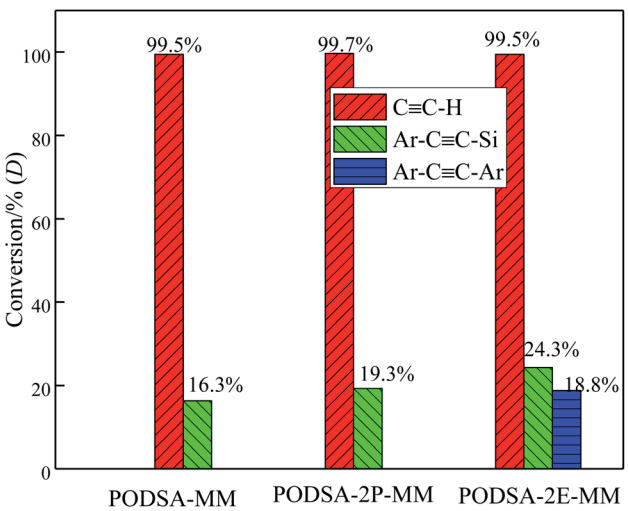

Fig. 9 The reaction degree of PODSA resins after curing.

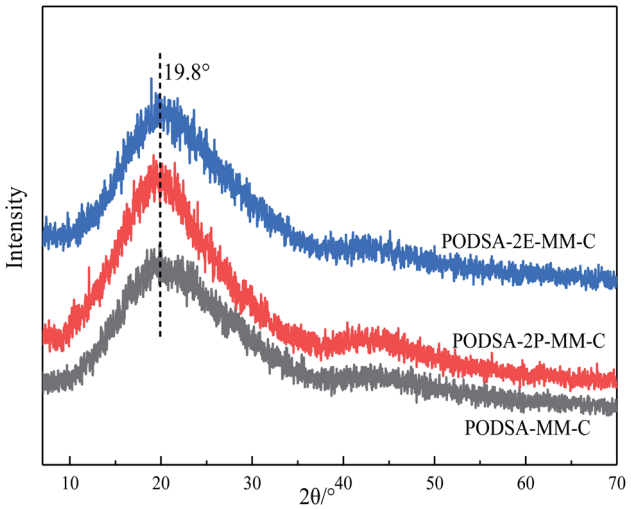

Fig. 10 The XRD diagrams of cured PODSA resins.

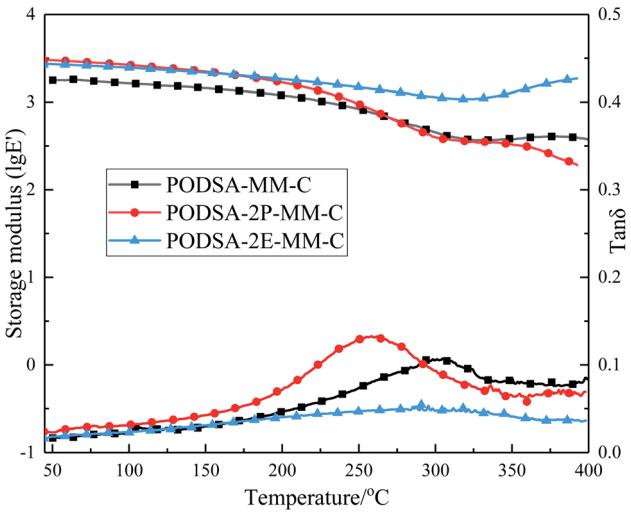

Fig. 11 The DMA curves of cured PODSA resins at the range of 40–400 °C.

reactions.[30] As can be seen in Fig. 10, there is no the sharp crystal peaks in the XRD pattern of the cured resins. The XRD patterns of three cured resins show similar phenomena. The XRD patterns of three cured resins show wide and slightly raised diffuse peak at the range of 10°–35°, and the locations of the highest peaks are 19.8° corresponding to the 20.7° for resins (Fig. 4A), indicating that the spatial structures are indeed affected and are short-range ordered structures at random orientation state. These results show that three cured resins have amorphous and uniform microstructures.

The mechanical properties of the cured resins. The cured resins were studied by dynamic thermal mechanical analysis in nitrogen flow at the range of 40–400 °C. The results are shown in Fig. 11. The storage modulus of three cured resins first decreases and then increases with the increasing of temperature due to the movement of molecular chains and thermal crosslinked reactions of acetylene groups at high temperature, respectively. The storage modulus of PODSA-2P-MM-C and PODSA-2E-MM-C are distinctly higher than that of PODSA-MM-C at low temperature, which are attributed to the fact that the movements of the main chains are restricted by the steric hindrance of side aromatic groups.[18,20] However, the storage modulus of PODSA-2P-MM-C decreases most obviously and hardly increases at high temperature due to the disturbance of side phenyl groups. PODSA-2E-MM-C do not show this behavior, and its storage modulus is always higher than that of PODSA-MM-C at the range of 40–400 °C. The loss factors of three cured resins are lower than 0.15 from 40 °C to 400 °C, and there is no glass transition temperature but there is a small relaxation peak over 250 °C, indicating that the thermal relaxation temperatures due to the mobilities of chain segments in the cured resins are high. The loss factor of PODSA-2P-MM-C is closely related with big free volume due to the π–π stacking between the rigid and polar structures and further curing reactions of internal acetylene groups in the main chain hindered by the side aromatic groups, resulting in the decrease of the thermal relaxation temperature.[17] However, for the PODSA-2E-MM-C, although it has a large free volume, the thermal crosslinking reactions of side phenylacetylene groups improve the structural stability, and significantly restrict the mobilities of chains at high temperature.

The mechanical properties of the cured resins at room temperature are summarized in Table 4. The flexural strength and modulus of PODSA-MM-C, PODSA-2P-MM-C, PODSA-2E-MM-C are 54.6 MPa, 38.1 MPa, 30.8 MPa and 2.4 GPa, 2.8 GPa, 3.3 GPa, respectively. The flexural strength of cured resins decrease and flexural modulus increase with the increase of volume of side aromatic group, which are attributed to the steric hindrance and thermal crosslinking reactions of side aromatic groups hindering the movements of the molecular chains and the less mechanical work dissipated by interchain slip, but increasing the energy barrier of the movements of the chain segments in the cured resins. These results indicate that the cured resins show poor mechanical properties due to side aromatic groups.

T300/PODSA composites were prepared and their mechanical properties are shown in Table 5. As shown in the table, the mechanical properties of the composites decrease with the appearance of the side aromatic groups, which are attributed to

Table 4 The mechanical properties of cured PODSA resins at room temperature

Sample	Flexural strength/MPa	Flexural modulus/GPa	Impact strength/kJ m^{-2}
PODSA-MM-C	54.6 ± 3.0	2.4 ± 0.3	10.2 ± 0.5
PODSA-2P-MM-C	38.1 ± 3.2	2.8 ± 0.1	4.9 ± 0.2
PODSA-2E-MM-C	30.8 ± 2.1	3.3 ± 0.1	2.5 ± 0.2

Table 5 The mechanical properties of T300 carbon fibre composites at room temperature

	Tensile strength/MPa	Tensile modulus/GPa	Flexural strength/MPa	Flexural modulus/GPa	ILSS/MPa
T300/PODSA-MM	445.2 ± 13.0	69.1 ± 5.3	550.2 ± 19.3	54.1 ± 3.3	37.5 ± 2.2
T300/PODSA-2P-MM	404.2 ± 15.5	64.8 ± 3.9	430.7 ± 24.3	53.5 ± 1.3	28.1 ± 2.1
T300/PODSA-2E-MM	383.1 ± 11.8	62.4 ± 5.0	341.6 ± 13.9	48.5 ± 1.1	20.2 ± 0.9

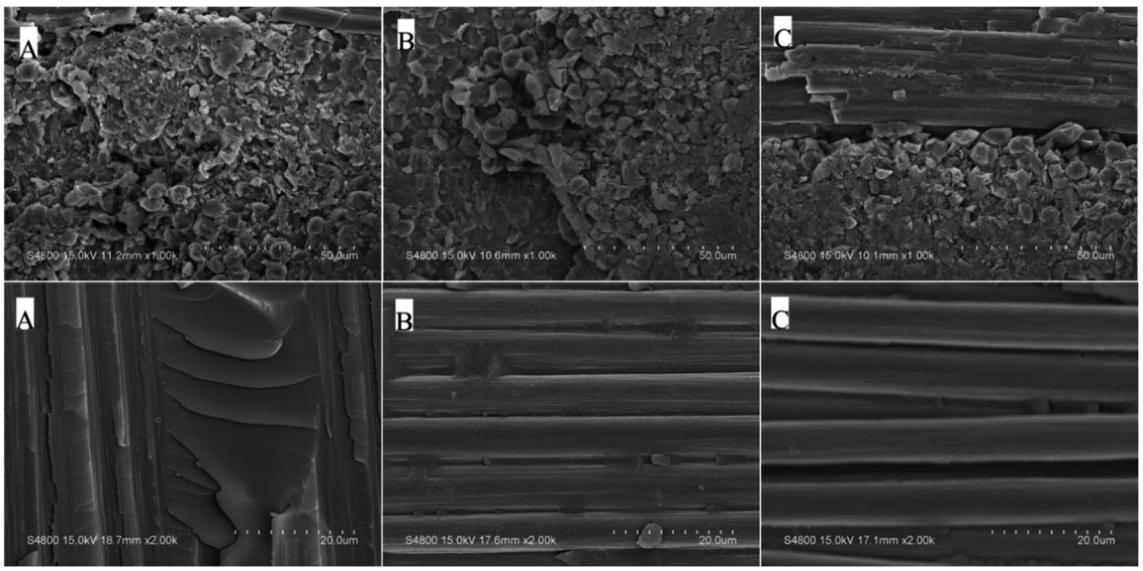

Fig. 12 The SEM photos with different magnifying powers for fracture surfaces of T300/PODSA-MM (A), T300/PODSA-2P-MM (B) and T300/PODSA-2E-MM (C) composites.

the weakening of the interfacial strength between the matrix and the fiber and the strength of the resins themselves. The SEM photos with different magnifying powers for fracture surfaces of T300/PODSA composites are shown in Fig. 12. There are resin fragments on the fracture surface of the composites, and the carbon fibers are wrapped in the matrix. With the size of side groups increasing in the resin, the less resin on the surface is left. These results show that the introduction of side aromatic groups weakens the interactions between the resin and the fiber, resulting in the decline of mechanical properties.

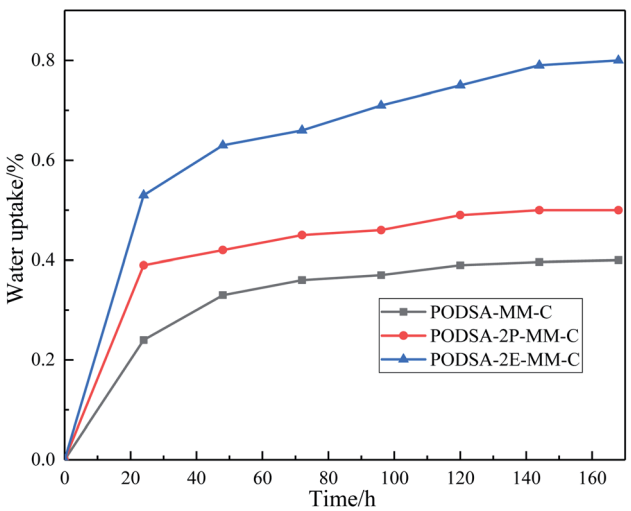

Fig. 13 The water uptake of the cured resins at room temperature.

The water uptake of the cured resins. The water uptakes of cured resins were explored at room temperature based on ASTM D 570–1998 standard.[17] The degrees of water absorption of cured resins are shown in Fig. 13. The water uptakes of three cured resins first increase rapidly, then slow down, and then maintain a stable value, the trends are similar to the common thermosets. The water absorptions of cured resins are less than 0.8 wt% after 160 h. With the increasing of volume of side aromatic groups, the water absorption capacities of the cured resins increase in the order of PODSA-MM-C < PODSA-2P-MM-C < PODSA-2E-MM-C, which could be attributed to large free volume caused by the hindrance of the side groups to the regular arrangement of the molecular chains. And the larger the side group is, the stronger the effect is. The densities of cured resins were measured by drainage method, and the results are tabulated in Table 6. The densities of cured resins decrease in the order of PODSA-MM-C > PODSA-2P-MM-C > PODSA-2E-MM-C, which is opposite to the change of water uptake, imply the

Table 6 The densities of the cured resins

Cured resin	PODSA-MM-C	PODSA-2P-MM-C	PODSA-2E-MM-C
Density/(g cm^{-3})	1.2106	1.1774	1.1737

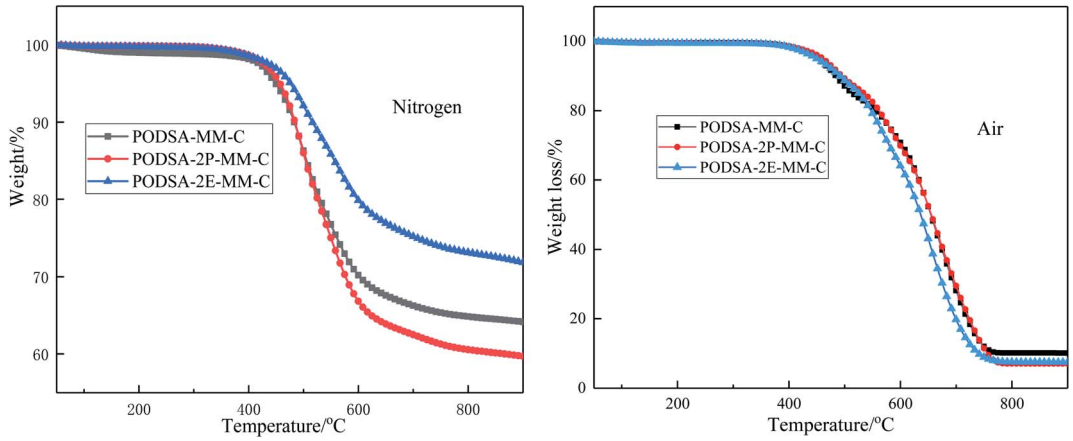

Fig. 14 The TGA curves of the cured resins in nitrogen and air.

Table 7 The TGA data of the cured resins

	Nitrogen		Air	
Sample	T_{d5}/°C	Y_{800}/%	T_{d5}/°C	Y_{800}/%
PODSA-MM-C	458	64.9	460	16.7
PODSA-2P-MM-C	466	60.6	470	7.0
PODSA-2E-MM-C	485	73.3	465	9.0

larger free volume in cured resins.[31] There results indicate that the increase of free volume in cured resin caused by side aromatic groups plays a dominant role in the change of water absorption and density.

The thermal stabilities of the cured resins. The results of thermal stabilities of three cured resins are shown in Fig. 14 and Table 7. The temperatures of 5% weight loss (T_{d5}) of PODSA-MM-C, PODSA-2P-MM-C and PODSA-2E-MM-C in nitrogen are 458 °C, 466 °C, 485 °C, respectively. And the T_{d5} of PODSA-MM-C, PODSA-2P-MM-C and PODSA-2E-MM-C in air are 460 °C, 470 °C, 465 °C, respectively. The cured resins have good thermal stabilities. The T_{d5} of cured resins are close in nitrogen and air due to the effects of 2,5-diphenyl-[1,3,4]-oxadiazole structure.[32] However, The T_{d5} of PODSA-2P-MM-C higher than that of PODSA-2E-MM-C in air may be due to the oxidative degradation of more acetylene groups and larger free volume.[33] The three cured resins have close reaction degrees, with the presence of side aromatic groups, but the percentage of [1,3,4]-oxadiazole structure in cured resins decrease,[17] thereby the T_{d5} of cured resins increase, because [1,3,4]-oxadiazole structure easily carry out pyrolysis reactions at high temperature. The residues of cured resins at 800 °C change in the order of PODSA-MM-C > PODSA-2E-MM-C > PODSA-2P-MM-C, which is attributed to the different silicon contents of resins and the thermal cross-linking reactions of the side phenylacetylene groups.

Conclusions

In conclusions, the silicon-containing arylacetylene resins with side aromatic phenyl and phenylacetylene groups (PODSA-MM, PODSA-2P-MM and PODSA-2E-MM) were synthesized by Grignard reactions of diynes with dimethyldichlorosilane, respectively. These resins have good processabilities and mild thermal cross-linking reactions. The rigid side aromatic groups strongly interfere with the regular degrees of the microstructures of the resins, the crystallization of the resins decrease according to the results of XRD and Raman analyses. As compared with the PODSA-MM resin without side groups, the novel resins exhibit wide processing windows, low crystallinity and exothermic enthalpy. The large free volume and chain movement ability restricted by steric hindrance of side aromatic groups lead to the corresponding cured resins show low densities and high modulus. And cured resins also have good heat resistance because of the low content of [1,3,4]-oxadiazole structure and thermal crosslinking reactions of side phenylacetylene groups. The works will provide guidance for obtaining high-performance composite matrix.

Conflicts of interest

There are no conflicts to declare.

Acknowledgements

The authors gratefully acknowledge the support of the Fundamental Research Funds for the Central Universities (no. JKD 01211701).

References

1 Z. Q. Wu, N. Li, J. H. Han, *et al.*, Low-viscosity and soluble phthalonitrile resin with improved thermostability for organic wave-transparent composites, *J. Appl. Polym. Sci.*, 2018, **135**, 45976.
2 M. Laskoski, D. D. Dominguez and T. M. Keller, Synthesis and properties of a liquid oligomeric cyanate ester resin, *Polymer*, 2006, **47**, 3727–3733.

3 Y. Z. Liu, Y. F. Liu, Y. G. Yang, *et al.*, Preparation and properties of graphene oxide–carbon fiber/phenolic resin composites, *Carbon*, 2013, **52**, 624.
4 M. Itoh, M. Mitsuzuka and K. Iwata, A novel synthesis and extremely high thermal stability of poly[(phenylsilylene) ethynylene-1,3phenyleneethynylene], *Macromolecules*, 1994, **27**, 7917–7919.
5 M. Itoh, K. Inoue, K. Iwata, *et al.*, New highly heat-resistant polymers containing silicon: poly(silyleneethynylenephenyleneethynylene)s, *Macromolecules*, 1997, **30**, 694–701.
6 M. Itoh, K. Iwata, M. Kobayashi, *et al.*, Preparations and properties of poly(vinylsilane)s, *Macromolecules*, 1998, **31**, 5609–5615.
7 M. Itoh, K. Inoue, N. Hirayama, *et al.*, Fiber reinforced plastics using a new heat-resistant silicon based polymer, *J. Mater. Sci.*, 2002, **37**, 3795–3801.
8 T. Ogasawara, Thermal response and ablation characteristics of carbon fiber reinforced composite with novel silicon containing polymer MSP, *Compos. Mater.*, 2002, **2**, 143–157.
9 M. P. Ma, Q. L. Yuan and F. R. Huang, A branched silicon-containing arylacetylene resin, *21st International Conference on Composite Materials*, 2017, p. 2928.
10 M. Itoh and K. Iwata, Various silicon-containing polymers with Si(H)–C≡C units, *J. Polym. Sci., Part A: Polym. Chem.*, 2001, **39**, 2658–2669.
11 F. Gao, L. L. Zhang, F. R. Huang, *et al.*, Synthesis and characterization of poly(tetramethyldisiloxane-ethynylenephenyleneethynylene) resins, *J. Polym. Res.*, 2011, **18**, 163–169.
12 F. Wang, J. F. Xu, J. Zhang, *et al.*, Synthesis and thermal of diphenyl ethers terminated with acetylene and phenylacetylene, *Polym.Int.*, 2006, **55**, 1063–1068.
13 F. F. Li, C. F. Wang, X. N. Shen, *et al.*, Synthesis and characterization of novel silicon-containing aromatic bispropargyl ether resins and their composites, *Polym. J.*, 2011, **43**, 594–599.
14 H. G. Chen, H. Xin, J. R. Lu, *et al.*, Synthesis and properties of poly(dimethylsilylene-ethynylenephenoxyphenoxyphenylene-ethynylene), *High Perform. Polym.*, 2017, **29**, 595–601.
15 M. P. Ma, Q. L. Yuan, F. R. Huang, *et al.*, Synthesis and properties of a silicon-containing arylacetylene resin with 2,6-diphenoxypyridine unit, *ChemistrySelect*, 2020, **5**, 1146–1152.
16 C. Li, J. W. Luo, M. P. Ma, *et al.*, Synthesis and properties of sulfur-contained poly(silylene arylacetylene) s, *J. Polym. Sci., Part A: Polym. Chem.*, 2019, **57**, 2324–2332.
17 M. P. Ma, C. J. Gong, C. Li, *et al.*, The synthesis and properties of silicon-containing arylacetylene resins with rigid-rod 2,5-diphenyl-[1,3,4]-oxadiazole moieties, *Eur. Polym. J.*, 2021, **143**, 110192.
18 H. Jiang, L. Sun, Y. R. Zhang, *et al.*, Estrogenic activity research of a novel fluorinated bisphenol and preparation of an epoxy resin as alternative to bisphenol A epoxy resin, *Eur. Polym. J.*, 2018, **108**, 507–516.
19 R. W. Lenz, A. Furukawa, P. Bhowmik, *et al.*, Synthesis and characterization of extended rod thermotropic polyesters with polyoxyethylene pendant substituents, *Polymer*, 1991, **32**, 1703–1712.
20 D. O. Kim and C. D. Han, Effect of bulkiness of pendent side groups on the rheology of semiflexible main-chain thermotropic liquid-crystalline polymers, *Macromolecules*, 2000, **33**, 3349–3358.
21 M. Li, Q. B. Guan and T. J. Dingemans, High-temperature shape memory behavior of semicrystalline polyamide thermosets, *ACS Appl. Mater. Interfaces*, 2018, **10**, 19106–19115.
22 C. Y. Wang, Y. P. Zhou, B. Shen, *et al.*, Proton-conducting poly(ether sulfone ketone)s containing a high density of pendant sulfonic groups by a convenient and mild post-sulfonation, *Polym. Chem.*, 2018, **9**, 4984–4993.
23 S. Y. Son, J. H. Kim, T. Park, *et al.*, Exploiting π-π stacking for stretchable semiconducting polymers, *Macromolecules*, 2018, **51**, 2572–2579.
24 J. A. Mikroyannidis, Synthesis by heck coupling of soluble, blue-light-emitting fully conjugated poly(*p*-phenylenevinylene)s with highly phenylated side groups, *Macromolecules*, 2002, **35**, 9289–9295.
25 T. Takada, S. Ishino, A. Takata, *et al.*, Rapid electron transfer of stacked heterodimers of perylene diimide derivatives in a DNA duplex, *Chem.–Eur. J.*, 2018, **24**, 8228–8232.
26 L. Chen, H. B. Zhao, Y. P. Ni, *et al.*, 3D printable robust shape memory PET copolyesters with fire safety *via* π-stacking and synergistic crosslinking, *J. Mater. Chem. A*, 2019, **7**, 17037–17045.
27 E. Romano, N. Anahi, R. Rudyk, *et al.*, Theoretical study of the infrared spectrum of 5-phenyl-1,3,4-oxadiazole-2-thiol by using DFT calculations, *Mol. Simul.*, 2012, **38**, 561–566.
28 J. Monni, P. Niemel, L. Alvila, *et al.*, Online monitoring of synthesis and curing of phenol-formaldehyde resol resins by Raman spectroscopy, *Polymer*, 2008, **49**, 3865–3874.
29 J. W. Luo, X. T. Liu, M. P. Ma, *et al.*, Dendritic poly(silylene arylacetylene) resins based on 1,3,5-triethynylbenzene, *Eur. Polym. J.*, 2020, **129**, 109628.
30 I. Jeong, C. B. Kim, D. G. Kang, *et al.*, Liquid crystalline epoxy resin with improved thermal conductivity by intermolecular dipole-dipole interactions, *J. Polym. Sci., Part A: Polym. Chem.*, 2019, **57**, 708–715.
31 O. Becker, Y. Cheng, R. J. Varley, *et al.*, Layered silicate nanocomposites based on various high-functionality epoxy resins: the influence of cure temperature on morphology, mechanical properties, and free volume, *Macromolecules*, 2003, **36**, 1616–1625.
32 J. A. Mikroyannidis, K. M. Gibbons, A. P. Kulkarni, *et al.*, Poly(fluorenevinylene) copolymers containing bis(phenyl) oxadiazole and triphenylamine moieties: synthesis, photophysics, and redox and electroluminescent properties, *Macromolecules*, 2008, **41**, 663–674.
33 N. Slavinskaya, A. Mirzayeva, R. Whitside, *et al.*, A modelling study of acetylene oxidation and pyrolysis, *Combust. Flame*, 2019, **210**, 25–42.